Subgap two-particle spectral weight in disordered *s*-wave superconductors: Insights from mode coupling approach

Prathyush P. Poduval,[1,*] Abhisek Samanta,[2,†] Prashant Gupta,[3,4] Nandini Trivedi,[5] and Rajdeep Sensarma[6,‡]

[1]*Indian Institute of Science, Bangalore 560012, India*
[2]*Physics Department, Technion, Haifa 32000, Israel*
[3]*Department of Physics, University of Illinois, Chicago, Illinois 60607, USA*
[4]*UM-DAE Centre for Excellence in Basic Sciences (CEBS), Mumbai 400098, India*
[5]*Department of Physics, The Ohio State University, Columbus, Ohio 43201, USA*
[6]*Department of Theoretical Physics, Tata Institute of Fundamental Research, Mumbai 400005, India*

We study the two-particle spectral functions and collective modes of weakly disordered superconductors using a disordered attractive Hubbard model on a square lattice. We show that the disorder-induced scattering between collective modes leads to a finite subgap spectral weight in the long-wavelength limit. In general, the spectral weight is distributed between the phase and the Higgs channels, but as we move towards half filling the Higgs contribution dominates. The inclusion of the density fluctuations lowers the frequency at which this mode occurs and results in the phase channel gaining a larger contribution to this subgap mode. Near half filling, the proximity of the system to the charge density wave instability leads to strong fluctuations of the effective disorder at the commensurate wave vector ($[\pi, \pi]$). We develop an analytical mode coupling approach where the pure Goldstone mode in the long-wavelength limit couples to the collective mode at $[\pi, \pi]$. This provides insight into the location and distribution of the two-particle spectral weights between the Higgs and the phase channels.

I. INTRODUCTION

The superconductor-insulator transition in two-dimensional films as a function of disorder strength is one of the most studied quantum phase transitions in nature [1–3]. There is strong experimental [2–4] and theoretical evidence [5–7] that the transition is driven by the disordering of the phase of the Cooper pairs, rather than by weakening of the amplitude of their formation. Several interesting phenomena, including the existence of a single-particle gap [2,4], high-frequency inductive electric response [4], and high magnetoresistance [8] across the transition, support the idea that the Cooper pairs exist across the transition. Hence the focus naturally shifts to the properties of the two-particle spectral functions, which include the low-energy collective fluctuations of the superconducting order parameter. The fluctuations of the phase and the amplitude of the order parameter constitute the low-energy spectral weight in a clean superconductor. The long-wavelength amplitude mode, related to the Higgs excitation [9,10] of high-energy physics [11], has been observed through nonlinear spectroscopy [12–18].

A key observation from a recent experiment [19] is the availability of optical spectral weight well below the two-particle continuum in a disordered superconductor. The presence of this low-energy spectral weight together with

a hard single-particle gap was surprising. It is well known that in a clean superconductor, the long-wavelength collective mode occurs at zero frequency (Goldstone mode) and there is no spectral weight until one reaches the two-particle continuum threshold at twice the single-particle gap [10,20–22]. Recent theoretical work [23–26] which constructs the collective modes around the disordered mean-field solutions [5,27,28] of the Bogoliubov–de Gennes (BdG) theory has shown the presence of spectral weight of two-particle excitations at finite frequencies below the continuum threshold (see Fig. 1).

An important feature of the theoretical results is that the subgap weight of two-particle excitations exists even at the weakest disorder, showing that this is not a feature which can only be associated with the quantum phase transition, and that there is a nonperturbative (in disorder) redistribution of the spectral weight in the long-wavelength limit. The details of the subgap spectral weight, however, crucially depend on the approximations used in the theoretical calculations: In Refs. [23,26], the authors only considered the fluctuations of the pairing field and obtained a subgap feature which had a narrow spectral range and was dominated by the amplitude or Higgs component. In contrast, in Ref. [24], the authors also considered the fluctuations of the density field, but focused only on the $\mathbf{q} = [0, 0]$ spectral function, where they obtained broad spectral weights dominated by the phase mode.

In this paper, we understand the systematic trends of the subgap two-particle spectral weight in the weakly disordered *s*-wave superconductor using the disordered attractive Hubbard model on a square lattice as a prototype. To get analytic insights, we consider the mean-field saddle point of

*ppoduval@umd.edu
†abhiseks@campus.technion.ac.il
‡sensarma@theory.tifr.res.in
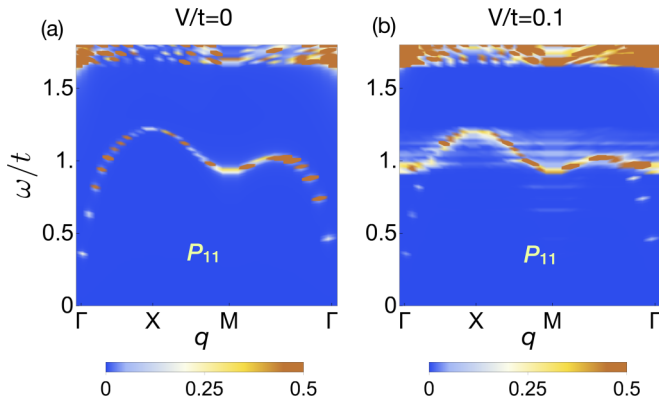
FIG. 1. The disorder-averaged amplitude spectral function $P_{11}(\mathbf{q}, \omega)$ for a system with (a) $V/t = 0$ corresponding to the clean case and (b) $V/t = 0.1$ corresponding to weak disorder. The spectral functions are calculated by expanding the action around the inhomogeneous BdG saddle point. In (b), a subgap mode is clearly seen at $\omega/t \sim 1$ around the Γ point ($\mathbf{q} = [0, 0]$). This is calculated for a 24×24 lattice with $U/t = 3$ and $n = 0.875$ (data taken from Ref. [23]). The single-particle gap of the clean superconductor is $\Delta_0/t = 0.83$. The continuum of the spectral weight for $P_{11}(\mathbf{q}, \omega)$ starts at $\omega = 2\Delta_0/t$.

the translation-invariant system (with no disorder) and expand the theory both in terms of static fluctuations created by the disorder and dynamic quantum fluctuations of the pairing and density fields. We thus obtain a description in terms of translation-invariant collective modes being scattered by an effective disorder. Using a simple Born approximation to account for the disorder scattering, we show that we can reproduce the subgap feature seen in earlier works. We also find that the static fluctuations are peaked around the commensurate vector of $\mathbf{Q} = [\pi, \pi]$, a reflection of the charge density wave (CDW) instability of the square lattice Hubbard model at half filling. Although the theoretical calculations are done away from half filling, the proximity effect causes this peak once the translation symmetry is broken by disorder. This motivates us to consider a simplified mode coupling theory, where the collective modes at $\mathbf{q}$ are coupled to those at $\mathbf{q} + \mathbf{Q}$.

Using this mode coupling theory, we show that the two-particle spectral weight at finite subgap frequencies at $\mathbf{q} = [0, 0]$ originates from the scattering of the $\mathbf{Q} = [\pi, \pi]$ mode by the effective disorder. Hence, at weak disorder, this weight appears around the energy of the $[\pi, \pi]$ mode in the clean system. We find that the particle-hole symmetry at half filling ensures that the Goldstone mode at $\mathbf{q} = [0, 0]$ couples only to the amplitude component of the $[\pi, \pi]$ mode, and hence the weight shows up only in the amplitude or Higgs channel close to half filling. As one moves away from half filling, the phase contribution to this subgap mode increases, as seen in the numerical calculations. The inclusion of dynamic density fluctuations [24] lowers the collective mode frequency at $[\pi, \pi]$. As a result, the subgap weight is shifted to lower frequencies, and the spectral separation between this mode and the tail of the low-energy weight from the Goldstone mode is lost. Furthermore, this lowering of the energy also implies that the subgap weight has a larger mixing of the pure phase Goldstone mode; thus the contribution of the phase component dominates in this case.

We note that if a disordered superconductor is close to a charge density wave transition, as in NbSe$_2$ [29], the strong static fluctuations at the commensurate wave vector will dominate the disorder scatterings. The presence of subgap spectral weight in the two-particle spectral function will also be a generic feature in that case. We note that unlike the work of Pekker and Varma [10] and Littlewood and Varma [20], where the system has additional CDW order, here the system is close to but not in the CDW phase. Hence, in a clean system, there will be no subgap weight at $\mathbf{q} = [0, 0]$. However, the presence of disorder, which breaks translational symmetry and allows for scattering of collective modes, leads to the formation of strong subgap spectral features in these systems.

To summarize, we have developed an analytical model of collective modes in weakly disordered superconductors which explains the following phenomena seen in earlier studies with detailed models [23,24,26]: (1) In a weakly disordered superconductor the collective mode spectrum consists of a subgap mode at $\mathbf{q} = 0$. Our model shows that the energy of this subgap mode is approximately the collective mode frequency of the clean superconductor at $\mathbf{Q} = [\pi, \pi]$. The strong static fluctuations at $\mathbf{Q}$ due to proximity to the CDW state leads to this subgap mode in the presence of disorder. (2) Near half filling, the mode is primarily in the amplitude channel, with the phase contribution increasing away from half filling. Our model shows that this is due to a particle-hole symmetry at half filling which leads to the vanishing of the relevant matrix elements. (3) Including density fluctuations pulls down the energy of the subgap mode at $\mathbf{q} = 0$. The softening of the collective mode at $\mathbf{Q}$ in the clean superconductor due to proximal CDW instability directly leads to the lowering of the subgap mode energy. This also increases the mixing between the Higgs component at $\mathbf{Q}$ and the phase-only Goldstone mode leading to a larger phase contribution to the subgap mode.

The rest of the paper is organized as follows: In Sec. II, we provide a summary of results on the two-particle spectral function of a weakly disordered attractive Hubbard model on a square lattice, obtained from numerical calculations using BdG theory and expansions around this inhomogeneous saddle point. In Sec. III, we expand the theory around the translation-invariant saddle point in both the disorder-induced static spatial fluctuations and the dynamic quantum fluctuations. This leads to a model of translation-invariant collective modes scattered by an effective disorder. We show that a simple Born approximation can reproduce the subgap spectral weight. In Sec. IV, we derive an approximate mode coupling theory by focusing on the fact that the nearby CDW instability leads to a peak in the static correlators at the corresponding commensurate wave vector (here, $[\pi, \pi]$). We then use this mode coupling theory to understand the systematic trends in the numerical calculations around the inhomogeneous mean-field solutions. We finally conclude by summarizing in Sec. V.

II. COLLECTIVE MODES IN DISORDERED SUPERCONDUCTORS: RESULTS FROM FERMIONIC THEORY

In this section we will review the results on collective modes of disordered s-wave superconductors obtained from a

theory of fermions with attractive interactions in the presence of a random disorder potential. This will give us the key phenomenology which we want to explain; at the same time, it will help in setting up the basic theoretical framework that we will use in the rest of the paper. Some of these results have been previously reported in Refs. [23–26].

We work with the attractive Hubbard model on a square lattice, with random potential disorder at zero temperature, given by the Hamiltonian

$$H = -t \sum_{\langle rr' \rangle \sigma} (c_{r\sigma}^\dagger c_{r'\sigma} + \text{H.c.}) - U \sum_r n_{r\uparrow} n_{r\downarrow}$$
$$+ \sum_r (v_r - \mu) n_r, \tag{1}$$

where $c_{r\sigma}^\dagger$ ($c_{r\sigma}$) is the creation (annihilation) operator for an electron with spin σ on site r, and μ is the chemical potential. Here, t is the nearest-neighbor hopping parameter, and U is the local attractive interaction between the electrons. v_r is an independent random variable for each site that is uniformly sampled from $[-V/2, V/2]$; thus V characterizes the scale of the disorder. We note that our model neglects the long-range Coulomb interactions and works only with the strong short-range attraction. While the effect of long-range Coulomb interaction on collective modes [30–33] is interesting in its own right, our main goal here is to provide insights into the phenomena seen in Refs. [23,24], both of which use only short-range interactions to describe the disordered superconductor.

The first step is to construct a mean-field theory in terms of the pairing field $\Delta_0(r) = U \langle c_{r\uparrow}^\dagger c_{r\downarrow}^\dagger \rangle$ and the Hartree shift $\xi_0(r) = U \langle c_{r\sigma}^\dagger c_{r\sigma} \rangle$. This leads to the mean-field Bogoliubov–de Gennes Hamiltonian

$$\begin{pmatrix} H_0(rr') & \Delta_0(r)\delta_{rr'} \\ \Delta_0(r)\delta_{rr'} & -H_0(rr') \end{pmatrix} \begin{pmatrix} u_m(r') \\ v_m(r') \end{pmatrix} = E_m \begin{pmatrix} u_m(r) \\ v_m(r) \end{pmatrix}, \tag{2}$$

where $H_0(rr') = -t_{rr'} - [\mu - v^{\text{eff}}(r)]\delta_{rr'}$ if r and r' are either nearest neighbors or the same site, and 0 otherwise. Here, $t_{rr'} = t$ if r and r' are nearest neighbors, and 0 otherwise. The microscopic disorder potential v_r is renormalized by the Hartree shift to the effective disorder potential $v^{\text{eff}}(r) = v_r - \xi_0(r)$. We note that while v_r is an independent random variable for each site, $\Delta_0(r)$ and $v^{\text{eff}}(r)$ for different sites have finite correlations between them. The self-consistent mean-field equations at zero temperature are then given by

$$\Delta_0(r) = U \sum_{m:E_m>0} u_m(r)v_m(r),$$
$$\xi_0(r) = U \sum_{m:E_m>0} v_m^2(r). \tag{3}$$

Additionally, we fix the average density of each disorder configuration to n by solving the number equation $n = \frac{2}{N_s} \sum_r \sum_{m:E_m>0} v_m^2(r)$. It is well known from earlier works [5,34,35] that the distributions of $\Delta_0(r)$ and $v^{\text{eff}}(r)$ change from a narrow distribution around the mean value at low disorders to bimodal distributions indicating the formation of superconducting and nonsuperconducting patches in the system at strong disorder.

The collective modes in disordered superconductors arise from the spatiotemporal *fluctuations* of the pairing field about the inhomogeneous mean-field solution. In an imaginary time (τ) formalism, this is achieved by considering $\Delta(r, \tau) = (\Delta_0(r) + \eta(r, \tau))e^{i\theta(r,\tau)}$, where $\eta(r, \tau)$ is the amplitude and $\theta(r, \tau)$ is the phase fluctuation. Expanding the action to second order in these fluctuation fields, one obtains a noninteracting theory (quadratic action) of the amplitude and phase fluctuations,

$$S = \sum_{rr', \omega_n} (\eta(r, i\omega_n), \theta(r, i\omega_n)) \hat{D}^{-1}(r, r', i\omega_n) \begin{pmatrix} \eta(r', -i\omega_n) \\ \theta(r', -i\omega_n) \end{pmatrix}, \tag{4}$$

where the details of the 2×2 matrix inverse propagator $\hat{D}^{-1}$ are given in Ref. [23]. The experimentally measurable amplitude spectral function is given by the analytic continuation to real frequencies, $P_{11}(r, r', \omega) = -\frac{1}{\pi} \text{Im} D_{11}(r, r', i\omega_n \to \omega + i0^+)$, while the corresponding phase spectral function is given by $P_{22}(r, r', \omega) = -\frac{1}{\pi} \Delta_0(r)\Delta_0(r') \text{Im} D_{22}(r, r', i\omega_n \to \omega + i0^+)$. In a disordered system, the spectral functions, calculated for a particular disorder configuration, do not have translational invariance. However, translation invariance is restored on disorder averaging, so that the disorder-averaged spectral function can be Fourier transformed in spatial coordinates. These disorder-averaged spectral functions, $P_{11}(\mathbf{q}, \omega)$ and $P_{22}(\mathbf{q}, \omega)$, have been studied in detail previously as a function of disorder at zero temperature [23,24] and at finite temperatures [26]. In this paper, we will only present results for zero temperature.

An intriguing result from Ref. [23] is the dramatic change in the low-energy Higgs (amplitude) spectral function at weak disorder. In the clean case, it is well known that the linearly dispersing collective mode has a pure phase character as $\mathbf{q} \to [0, 0]$, i.e., the amplitude component goes to 0. At $\mathbf{q} = [0, 0]$, the Higgs spectral weight resides at the two-particle continuum threshold, and the mode is damped out. In contrast, even at very weak disorder, there are sharply defined excitation modes (peaks in spectral function) in the Higgs channel below the two-particle continuum in the long-wavelength limit ($\mathbf{q} = [0, 0]$). In Fig. 1, we show color plots of the amplitude spectral function $P_{11}(\mathbf{q}, \omega)$ in the $\mathbf{q}$-ω plane (with $\mathbf{q}$ along the principal axes in the Brillouin zone), calculated from such a Gaussian expansion around the mean-field theory at $U/t = 3$ and $n = 0.875$. Figure 1(a) shows the clean case ($V/t = 0$), where the Higgs weight at $\mathbf{q} = [0, 0]$ (Γ point) starts from the two-particle continuum threshold. Figure 1(b) shows the spectral function at a weak disorder of $V/t = 0.1$. In this case, it is clear that at $\mathbf{q} = [0, 0]$, the amplitude spectral function has finite weight at an energy ω_0, which is below the two-particle gap $2\Delta_0$. Surprisingly, the weight at $\mathbf{q} = [0, 0]$ is observed only over a narrow band of frequencies close to the collective mode frequency at $\mathbf{Q} = [\pi, \pi]$, which suggests that the weight signifies an actual quasiparticle excitation. This is unlikely to be caused just by the incoherent scatterings from the disorder potential and suggests the existence of a more fundamental mechanism. In addition, we also see a small but finite low-energy weight near the M point, which was absent in the clean case. We note that we will present data for $U/t = 3$ in this paper unless otherwise mentioned.
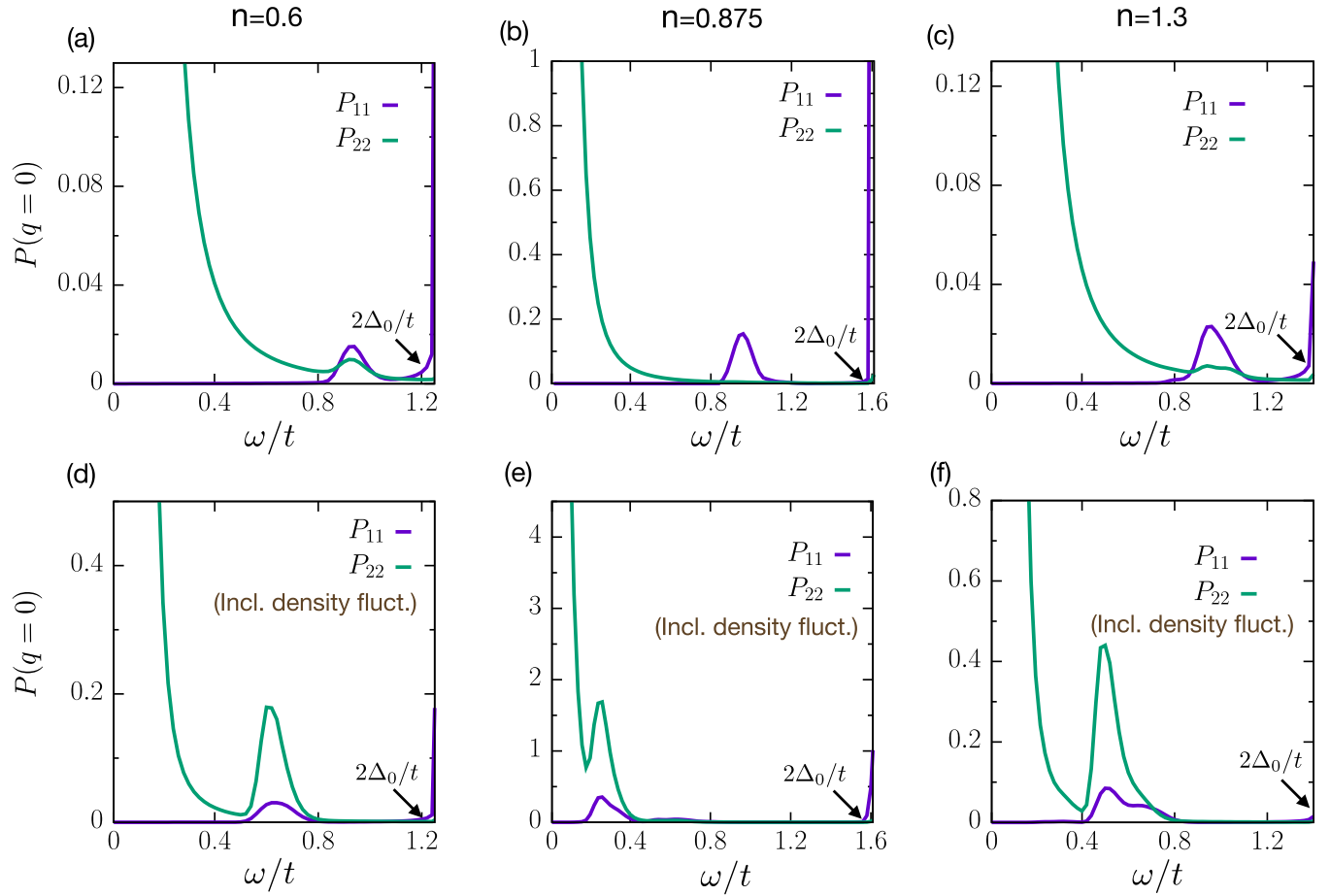
FIG. 2. The disorder-averaged energy distribution curves (EDCs) for amplitude and phase spectral functions (P_{11} and P_{22}) for $\mathbf{q} = [0, 0]$ for different densities: (a) and (d) $n = 0.6$, (b) and (e) $n = 0.875$, and (c) and (f) $n = 1.3$. (a)–(c) show the spectral functions without the effects of dynamic density fluctuations [23], and (d)–(f) show the spectral functions after including the effects of dynamic density fluctuations (Incl. density fluct.) [24]. The results from expansion around the inhomogeneous saddle point show the following: (i) The phase contribution to the subgap mode increases as we move away from half filling on either side [(a)–(c)]. (ii) On including density fluctuations, the location of the subgap mode shifts to a lower value of ω, and the phase contribution to the subgap mode increases substantially [(d)–(f)]. All the data are for a 24×24 lattice with $U/t = 3$ and $V/t = 0.1$. The single-particle gaps of the corresponding clean superconductors are as follows: $\Delta_0/t = 0.65, 0.83, 0.74$ for $n = 0.6, 0.875, 1.3$, respectively. The continuum of the spectral weight starting at $\omega = 2\Delta_0/t$ is also indicated in the figure.

In order to understand the systematic changes in the long-wavelength spectral functions, we plot the energy distribution curves (EDCs) at $\mathbf{q} = [0, 0]$ for the amplitude and phase channel in Fig. 2. Figures 2(a), 2(b), and 2(c) show the results at a weak disorder of $V = 0.1t$ for three different densities, $n = 0.6, n = 0.875$, and $n = 1.3$, respectively. In all the cases, we see that the subgap spectral weight around ω_0 is spectrally well separated from the low-energy phase contribution of the collective mode. The spectral weight around ω_0 is exclusively in the Higgs channel at $n = 0.875$, whereas the weight is more evenly distributed between the amplitude and phase channels as we move away from half filling ($n = 0.6$ and $n = 1.3$). This seems to suggest that some approximate symmetry suppresses the phase contribution in this case as one approaches half filling.

Finally, in Ref. [24], the fluctuations of the Hartree (local density) field $\xi(r, \tau)$ were considered along with those of the pairing field. Expanding up to quadratic order, one gets an action similar to Eq. (4), now with a three-component field

(η, θ, ξ) and a 3×3 matrix propagator. The density fluctuations were then integrated out to obtain the effective collective modes for the η and θ fluctuations in the system. It was found that the subgap weight is shifted to much lower energy and overlaps with the spectral weight from the Goldstone (phase) mode. The systematic changes in the EDC on adding density fluctuations are shown in Figs. 2(d), 2(e), and 2(f) for densities $n = 0.6, 0.875$, and 1.3, respectively. Although the subgap mode does survive, its location and composition change drastically. Initially, the subgap mode was part of a flat band near the top of the collective mode spectrum. However, including the effects of density fluctuations causes the location of the mode to shift towards $\omega = 0$. Moreover, the composition of the subgap mode is dominated by the phase contributions.

To summarize, the following effects are seen in these calculations: (1) The presence of a weak disorder seems to give rise to an excitation at a finite ω below the two-particle continuum. (2) This mode is observed to be purely in the amplitude channel for $n \sim 0.875$, with the phase

contribution increasing both as we move away from half filling and when we include density fluctuations. (3) The location of this mode in ω space was initially part of a flat mode; however, it gets drastically pulled down when density fluctuations are included. While these trends are clear, it is hard to obtain additional insights from these calculations, since they can only be accessed by large-scale numerics. In the next section, we will formulate this problem in terms of the collective modes of the translation-invariant system interacting with an effective disorder to get additional insight into these trends.

III. COLLECTIVE BOSONS AND THEIR EFFECTIVE DISORDER

In the fermionic theory, the disorder is modeled by a random potential felt by the electrons at every site. The disorder strength (the width of the probability distribution of the random potential) can be related to experimentally observable quantities such as sheet resistance [4,36–38], and one can make a detailed comparison with realistic systems. However, there is a price to pay for this exact treatment of

the microscopic disorder. The eigenstates of the mean-field theory can only be determined numerically and vary from one disorder configuration to another. Hence calculations of collective modes are numerically expensive and are limited to small system sizes. Furthermore, it is hard to get any insight into the mechanisms behind the observed phenomena.

To circumvent these difficulties and obtain analytic insight into the subgap spectral weight, we obtain a description where the translation-invariant collective modes are scattered by an effective disorder. To achieve this, we note that within the mean-field BdG theory, the disorder gives rise to a local pairing $\Delta_0(r)$ and an effective local potential (microscopic disorder potential, renormalized by Hartree shifts) $v^{\text{eff}}(r)$. We can treat these as new random variables, which determine the properties of the mean-field solutions as well as the spectral properties of the collective modes. We break them up into an average (Δ_0 and v_0) and a static spatial fluctuation [$\delta\Delta_0(r) = \Delta_0(r) - \Delta_0$ and $\delta v(r) = v^{\text{eff}}(r) - v_0$]. Note that by construction, $\delta\Delta_0(r)$ and $\delta v(r)$ are correlated random variables with zero mean. We first consider a translation-invariant saddle point with Δ_0 and v_0, where the fermion Green's function in the Nambu basis in momentum space is given by

$$G(\mathbf{k}, i\omega_n) = \begin{pmatrix} \frac{u_{\mathbf{k}}^2}{i\omega_n - E_{\mathbf{k}}} + \frac{v_{\mathbf{k}}^2}{i\omega_n + E_{\mathbf{k}}} & u_{\mathbf{k}} v_{\mathbf{k}}\left[\frac{1}{i\omega_n - E_{\mathbf{k}}} - \frac{1}{i\omega_n + E_{\mathbf{k}}}\right] \\ u_{\mathbf{k}} v_{\mathbf{k}}\left[\frac{1}{i\omega_n - E_{\mathbf{k}}} - \frac{1}{i\omega_n + E_{\mathbf{k}}}\right] & \frac{v_{\mathbf{k}}^2}{i\omega_n - E_{\mathbf{k}}} + \frac{u_{\mathbf{k}}^2}{i\omega_n + E_{\mathbf{k}}} \end{pmatrix}, \tag{5}$$

where $\omega_n = (2n + 1)\pi T$ with integer n is the fermionic Matsubara frequency at temperature T. Here, $E_{\mathbf{k}} = \sqrt{(\epsilon_{\mathbf{k}} - \mu + v_0)^2 + \Delta_0^2}$ is the Bogoliubov quasiparticle dispersion, $\epsilon_{\mathbf{k}} = -2t(\cos k_x + \cos k_y)$ is the bare band dispersion, and the BCS coherence factors are given by $u_{\mathbf{k}}^2 = 1 - v_{\mathbf{k}}^2 = (1/2)(1 + (\epsilon_{\mathbf{k}} - \mu + v_0)/E_{\mathbf{k}})$ and $u_{\mathbf{k}} v_{\mathbf{k}} = \Delta_0/2E_{\mathbf{k}}$.

Our model of translation-invariant bosons coupled to effective disorder is obtained by considering $\Delta(r, \tau) = \Delta_0 + \delta\Delta(r) + \lambda(r, \tau)$ and $v(r, \tau) = v_0 + \delta v(r) + \xi(r, \tau)$ and expanding the action both in the dynamic quantum fluctuations [$\lambda(r, \tau), \xi(r, \tau)$] and in the disorder-induced static fluctuations $\delta\Delta(r)$ and $\delta v(r)$. This leads to the fluctuation action

$$S_{fl} = \frac{1}{2}\sum_{\mathbf{q},\omega_m} \Lambda^\dagger(\mathbf{q}, i\omega_m)\hat{M}^{-1}(\mathbf{q}, i\omega_m)\Lambda(\mathbf{q}, i\omega_m) + \sum_{\mathbf{q},\mathbf{q}_1,\omega_m} \Lambda^\dagger(\mathbf{q} + \mathbf{q}_1, i\omega_m)\hat{\hat{F}}(\mathbf{q}, \mathbf{q}_1, i\omega_m)\Lambda(\mathbf{q}, i\omega_m), \tag{6}$$

where $\omega_m = 2m\pi T$, with integer m, is the bosonic Matsubara frequency and the three-component field $\Lambda^\dagger(\mathbf{q}, i\omega_m) = [\lambda^*(\mathbf{q}, i\omega_m), \lambda(-\mathbf{q}, -i\omega_m), \xi(\mathbf{q}, i\omega_m)]$. We note that when we analyze the theory without density fluctuations, we will set $\xi = 0$ and work with a two-component field.

Here, $\hat{M}^{-1}$ is the inverse propagator for the translation-invariant collective modes,

$$M_{ij}^{-1}(\mathbf{q}, i\omega_m) = \frac{\delta_{ij}(1 + \delta_{i3})}{U} + \sum_{\mathbf{k},\omega_n} \text{Tr}\,^N G(\mathbf{k} + \mathbf{q}, i\omega_n + i\omega_m)\sigma^{\alpha_i} G(\mathbf{k}, i\omega_n)\sigma^{\beta_j}, \tag{7}$$

where the trace is over Nambu indices, $\alpha_i = +, -, 3$ for $i = 1, 2, 3$, respectively, and $\beta_j = -, +, 3$ for $j = 1, 2, 3$, respectively. Here, $\sigma^{i=1,2,3}$ denote the Pauli matrices, and $\sigma^{\pm} = \sigma^1 \pm i\sigma^2$. The detailed evaluation of M^{-1} is given in the Supplemental Material (SM) [39] (see also Refs. [21,22,24] for earlier derivations of the propagator). The low-energy poles of $\hat{M}(\mathbf{q}, \omega + i0^+)$ determine the collective mode frequencies of the translation-invariant system, which disperse linearly at low momenta. The second term in the action scatters a fluctuation at momentum $\mathbf{q}$ to a fluctuation at $\mathbf{q} + \mathbf{q}_1$ (with the same frequency) and is linearly dependent on the (Fourier transformed) static fluctuations $\delta\Delta_{\mathbf{q}_1}$ and $\delta v_{\mathbf{q}_1}$. The scattering matrix $\hat{\hat{F}}$ can be written as

$$\hat{\hat{F}}_{ij}(\mathbf{q}, \mathbf{q}_1, i\omega_m) = f_{ij}(\mathbf{q}, \mathbf{q}_1, i\omega_m)\delta\Delta_{-\mathbf{q}_1} + g_{ij}(\mathbf{q}, \mathbf{q}_1, i\omega_m)\delta v_{-\mathbf{q}_1}, \tag{8}$$

where i, j run between 1 and 3. The coupling functions are given by

$$f_{ij}(\mathbf{q}, \mathbf{q}_1, i\omega_m) = \sum_{\mathbf{k},\omega_n} \text{Tr}\,^N G(\mathbf{k} + \mathbf{q} + \mathbf{q}_1, i\omega_n + i\omega_m)\sigma^{\alpha_i} G(\mathbf{k}, i\omega_n)\sigma^1 G(\mathbf{k} + \mathbf{q}_1, i\omega_n)\sigma^{\beta_j},$$

$$g_{ij}(\mathbf{q}, \mathbf{q}_1, i\omega_m) = \sum_{\mathbf{k},\omega_n} \text{Tr}\,^N G(\mathbf{k} + \mathbf{q} + \mathbf{q}_1, i\omega_n + i\omega_m)\sigma^{\alpha_i} G(\mathbf{k}, i\omega_n)\sigma^3 G(\mathbf{k} + \mathbf{q}_1, i\omega_n)\sigma^{\beta_j}. \tag{9}$$
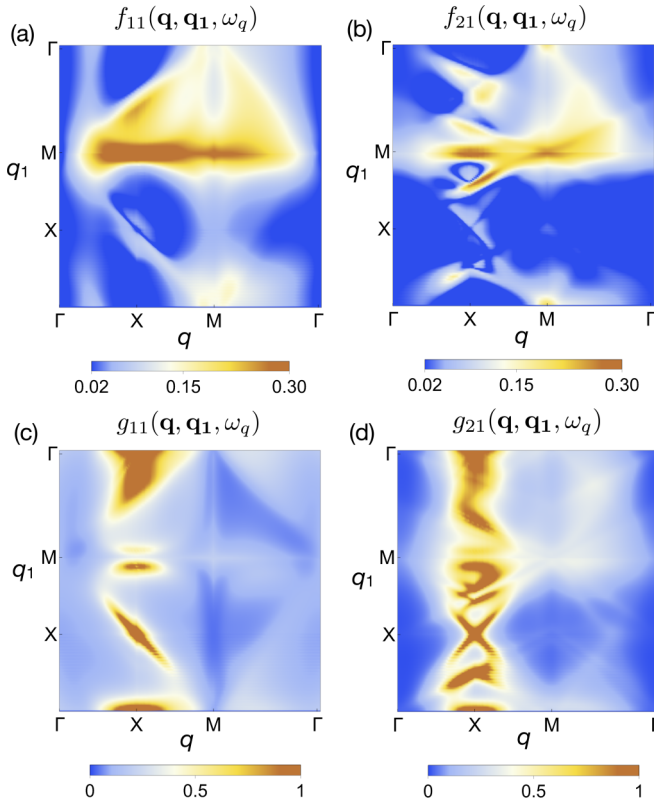
FIG. 3. The static fluctuations of the Hartree fields $\delta v_{\mathbf{q}_1}$ scatter the collective modes at momentum $\mathbf{q}$ to modes at $\mathbf{q} + \mathbf{q}_1$ with a coupling $f_{ij}(\mathbf{q}, \mathbf{q}_1, \omega_{\mathbf{q}})$, where $\omega_{\mathbf{q}}$ is the dispersion of the collective mode [see Eqs. (6) and (8)]. The color plots of f_{11} and f_{21} as a function of $\mathbf{q}$ and $\mathbf{q}_1$ along the principal axes are shown in (a) and (b), respectively. The corresponding couplings for static fluctuations of pairing fields $\delta \Delta_{\mathbf{q}_1}$, g_{11} and g_{21}, are shown in (c) and (d), respectively. f_{11} and f_{21} are relatively independent of $\mathbf{q}$ and are peaked around $\mathbf{q}_1 = M$. g_{11} and g_{21}, on the other hand, are independent of $\mathbf{q}_1$ but peaked around $\mathbf{q} = X$.

Other than the matrix structure, these terms have the general interpretation of an effective disorder scattering the collective modes at low energy. The explicit evaluation of the coupling functions $f_{\alpha\beta}$ and $g_{\alpha\beta}$ is shown in the SM [39]. For real frequencies below the two-particle continuum, these coupling functions are real. Since we are interested in the scattering of the collective modes due to disorder, the coupling of interest to us is obtained by considering the analytic continuation $i\omega_m \to \omega_{\mathbf{q}} + i0^+$, where $\omega_{\mathbf{q}}$ is the collective mode frequency at $\mathbf{q}$. These couplings are the amplitude for scattering a collective mode at $\mathbf{q}$ by a momentum $\mathbf{q}_1$. In Fig. 3(a), we plot $f_{11}(\mathbf{q}, \mathbf{q}_1, \omega_{\mathbf{q}})$ as a color plot in the $\mathbf{q}$-$\mathbf{q}_1$ plane (with momenta taken along principal axes of the Brillouin zone). We find that the coupling is peaked around the momentum transfer of $\mathbf{q}_1 = Q = [\pi, \pi]$, while it is reasonably independent of the starting wave vector $\mathbf{q}$. In Figs. 3(b)–3(d), we plot the coupling functions f_{21}, g_{11}, and g_{21}, respectively. We find that f_{11} and f_{21} have similar dependence on momenta. In contrast, g_{11} and g_{21} are very sensitive to $\mathbf{q}$, peaking around $\mathbf{q} = X = [\pi, 0]$, and are relatively independent of $\mathbf{q}_1$, the momentum transferred in the scattering. The scattering of the quantum fluctuations around the translation-invariant saddle point by

the static disorder can be represented in terms of Feynman diagrams, with fluctuation propagators and vertices coupling the dynamic fluctuations to the static effective disorder, as shown in Fig. 4. We note that this action is derived to leading order in the static fluctuations and hence would fail to account for higher-order scatterings at strong disorder. However, we are only interested in the properties of the collective modes at weak disorder; so this provides a sufficient starting point to understand the phenomenology described in Sec. II.

After constructing the effective action for the collective bosons and their scattering due to disorder, we need an approximate way to incorporate the effects of these scatterings into the spectral function of the fluctuations. This is done by dressing the inverse propagator M^{-1} by the self-energies due to disorder scattering $M^{-1} \to M^{-1} - \Sigma$ and constructing the imaginary part of the propagator obtained from this dressed Green's function for the fluctuations. For this, we use the simplest Born approximation scheme (the self-energy diagrams are shown in Fig. 4), where the self-energy matrix can be written as

$$\hat{\Sigma}(\mathbf{q}, i\omega_m) = \sum_{\mathbf{q}_1} \hat{\bar{F}}_{\mathbf{q}+\mathbf{q}_1, -\mathbf{q}_1, i\omega_m} \hat{M}_{\mathbf{q}+\mathbf{q}_1, i\omega_m} \hat{\bar{F}}_{\mathbf{q}, \mathbf{q}_1, i\omega_m}. \quad (10)$$

We note that there is a self-energy term linear in $\hat{F}$, which vanishes on averaging over disorder, leaving this as the leading-order contribution. The Born approximation is valid at weak disorder and will fail to capture nonperturbative effects due to disorder scattering. To see the effectiveness of our approximations in capturing the phenomena described in the previous section, we consider the static correlators

$$\langle |\delta\Delta(\mathbf{q})|^2 \rangle = \frac{1}{N_s} \sum_{r,r'} e^{i\mathbf{q}(r-r')} \langle \delta\Delta(r)\delta\Delta(r') \rangle,$$

$$\langle |\delta v(\mathbf{q})|^2 \rangle = \frac{1}{N_s} \sum_{r,r'} e^{i\mathbf{q}(r-r')} \langle \delta v(r)\delta v(r') \rangle, \quad (11)$$

$$\langle \delta v(\mathbf{q})\delta\Delta(-\mathbf{q}) \rangle = \frac{1}{N_s} \sum_{r,r'} e^{i\mathbf{q}(r-r')} \langle \delta v(r)\delta\Delta(r') \rangle,$$

where N_s is the number of sites in the system and the correlators are calculated in the inhomogeneous BdG solutions of the disordered system. Here, the averaging is over disorder realizations. These correlators then give the disorder-averaged self-energy, which is used to construct the spectral functions of the fluctuations.

We first consider a superconductor at a density $n = 0.875$ at a weak disorder $V/t = 0.1$ on a 24×24 lattice. We suppress the quantum density fluctuations and work in the two-component formalism. The spectral functions for the λ fluctuations in this case are plotted in Fig. 5. For a system with $U/t = 3$, Fig. 5(a) shows the spectral function corresponding to $\langle \lambda_{\mathbf{q}} \lambda_{\mathbf{q}}^* \rangle$, while Fig. 5(b) shows spectral weights in $\langle \lambda_{\mathbf{q}}^* \lambda_{-\mathbf{q}}^* \rangle$. Figures 5(c) and 5(d) show the corresponding plots for $U/t = 4$. We see that the $U/t = 4$ data clearly show the formation of a flat mode leading to a narrow subgap weight at $\mathbf{q} = [0, 0]$ at a finite frequency. The upper edge of the collective modes at $U/t = 3$ are too close to the continuum to see this clearly. Here, we would like to note that the dispersion of the large-momentum, high-frequency collective mode depends on
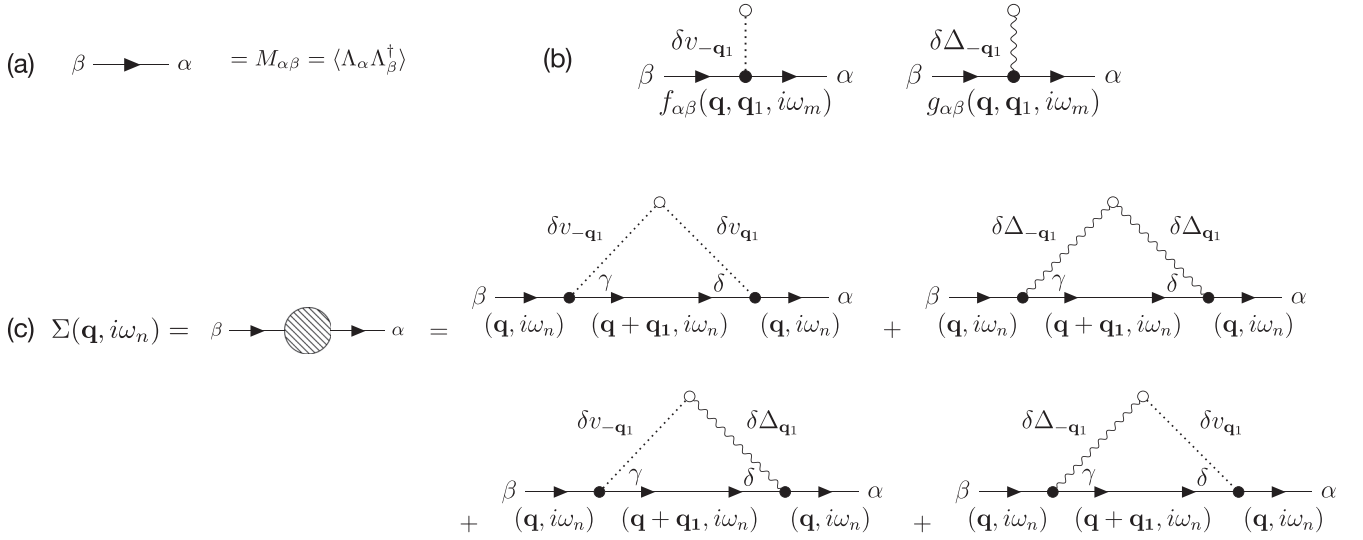
FIG. 4. The Feynman diagrams for the self-energy of the collective modes due to scattering by the static fluctuations. (a) The line denoting the propagator of quantum fluctuations. (b) The Feynman vertices that couple the static fluctuations with the dynamic fluctuations. (c) The self-energy diagrams in the leading-order Born approximation. The self-energy terms are proportional to $\langle |\delta\Delta(\mathbf{q})|^2\rangle$, $\langle |\delta v(\mathbf{q})|^2\rangle$, and $\langle \delta v(\mathbf{q})\delta\Delta(-\mathbf{q})\rangle$.
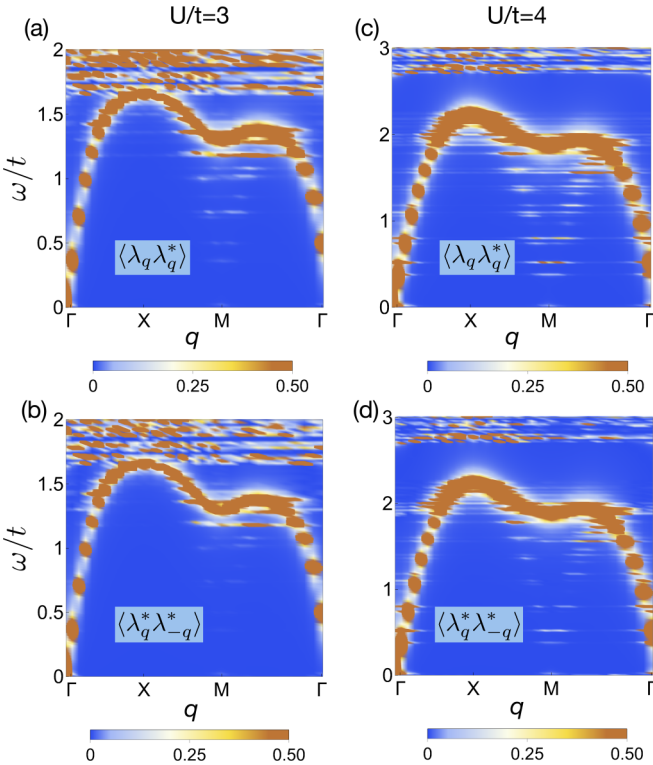
FIG. 5. The fluctuation spectral functions calculated within the Born approximation with effective disorder obtained from mean-field BdG solutions for (a) and (b) $U/t = 3$ and (c) and (d) $U/t = 4$. Here, we use the Cartesian form of the fluctuations. (a) and (c) give the diagonal part of the spectral function, and (b) and (d) give the off-diagonal parts. There is a small pileup of weight at $\mathbf{q} = [0, 0]$ signifying the formation of a subgap mode.

whether one uses a "Cartesian" representation of fluctuations (as done here) or works with the amplitude-phase representation. In the amplitude-phase representation, the collective mode frequencies are a bit lower than and better separated from the two-particle continuum. There is also pileup of low-energy weight observed near the M point. This shows that this simple approximation is able to capture the occurrence of subgap two-particle spectral weight at long wavelengths in a weakly disordered superconductor. In the next section, we will work in the amplitude-phase coordinates and further simplify our model to obtain an analytic understanding of the systematic trends in the two-particle spectral functions at weak disorder.

IV. CDW FLUCTUATIONS AND EFFECTIVE TWO-BAND MODEL

In the previous section, we have converted the problem of attractive fermions in the presence of a disorder potential to that of bosonic collective fluctuations of the superconducting order parameter scattered by an effective disorder in pairing amplitudes and local potentials. We have also seen that a Born approximation calculation using the variance and co-variance of the effective disorder fields obtained from BdG solutions reproduces the basic phenomena of a narrow subgap weight below the continuum threshold at $\mathbf{q} = [0, 0]$. In order to make further analytic progress, we need an analytic handle on the static fluctuation correlators, $\langle |\delta v(\mathbf{q})|^2\rangle$, $\langle |\delta\Delta(\mathbf{q})|^2\rangle$, and $\langle \delta v(\mathbf{q})\delta\Delta(-\mathbf{q})\rangle$.

In this section, we show that the static fluctuation correlators are strongly peaked at $\mathbf{q} = [\pi, \pi]$ near half filling and the peak broadens as we move away from half filling. Moreover,
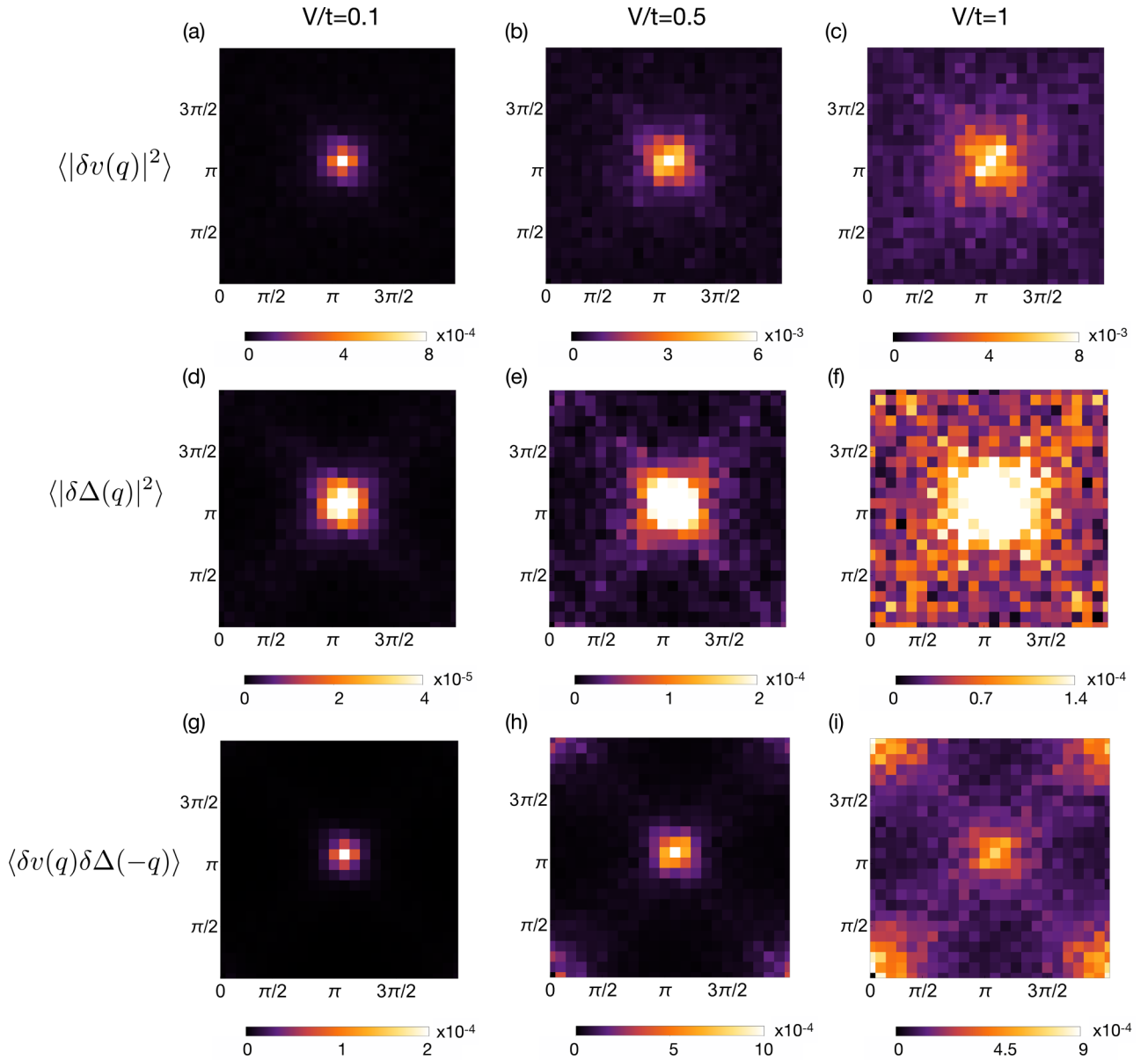
FIG. 6. The disorder-averaged static fluctuations of (a)–(c) the Hartree field $\langle|\delta v(\mathbf{q})|^2\rangle$, with $V/t = 0.1$ (a), 0.5 (b), and 1.0 (c); (d)–(f) the pairing field $\langle|\delta\Delta(\mathbf{q})|^2\rangle$, with $V/t = 0.1$ (d), 0.5 (e), and 1.0 (f); and (g)–(i) the cross correlator $|\langle\delta v(\mathbf{q})\delta\Delta(-\mathbf{q})\rangle|$, with $V/t = 0.1$ (g), 0.5 (h), and 1.0 (i) over the full two-dimensional (2D) Brillouin zone. This is calculated from BdG solutions on a 24×24 lattice in a system with $U/t = 3$, $n = 0.875$ and averaged over 15 disorder realizations. The Hartree correlator is very strong at (π, π) and then spreads out around this point as the disorder strength is increased. The superconducting correlators follow a similar pattern; however, the corresponding magnitudes are about a factor of 10 smaller than those of Hartree correlators.

the density correlator $\langle|\delta v(\mathbf{q})|^2\rangle$ is found to be much larger than $\langle|\delta\Delta(\mathbf{q})|^2\rangle$ and $\langle\delta v(\mathbf{q})\delta\Delta(-\mathbf{q})\rangle$. Using this, we construct an effective model considering only a scattering between fluctuating superconducting modes at $\mathbf{q}$ and $\mathbf{q} + \mathbf{Q}$, mediated only by the static density fluctuation. Within this simplified two-band model, we can recover the trends in the distribution of the spectral weight of the subgap mode between the amplitude, phase, and density channels as we move away from half filling. Moreover, we analytically show the dominance of the phase mode near half filling due to approximate particle-hole symmetry.

We consider a system with $U/t = 3$ and $n = 0.875$ and plot the correlators $\langle|\delta v(\mathbf{q})|^2\rangle$, $\langle|\delta\Delta(\mathbf{q})|^2\rangle$, and $\langle\delta v(\mathbf{q})\delta\Delta(-\mathbf{q})\rangle$, calculated from the spatially inhomogeneous mean-field solutions. Figures 6(a), 6(b), and 6(c) show color plots of the effective potential correlator $\langle|\delta v(\mathbf{q})|^2\rangle$ as a function of $\mathbf{q}$ for increasing disorder strengths $V/t = 0.1$, 0.5, and 1.0, respectively. Figures 6(d)–6(f) show the corresponding plots for $\langle|\delta\Delta(\mathbf{q})|^2\rangle$, and Figs. 6(g)–6(i) show the cross correlator between the pairing amplitude and the effective potential. Two interesting trends can be seen in these plots: (a) $\langle|\delta v(\mathbf{q})|^2\rangle \gg \langle|\delta\Delta(\mathbf{q})|^2\rangle$, $\langle\delta v(\mathbf{q})\delta\Delta(-\mathbf{q})\rangle$, so that it is
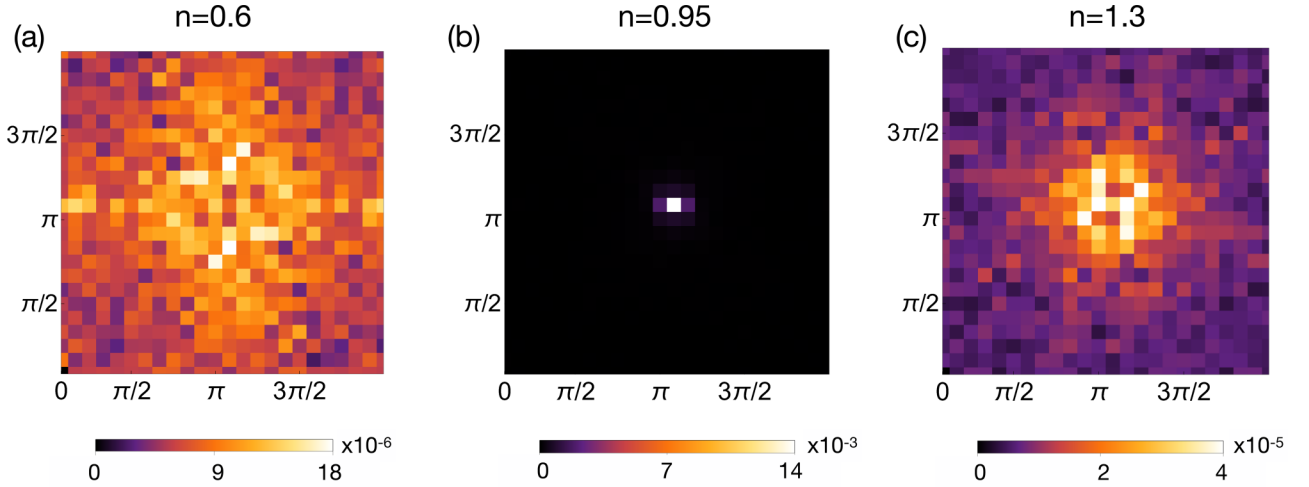
FIG. 7. Color plots of the disorder-averaged static fluctuations of the Hartree field $\langle |\delta v(\mathbf{q})|^2 \rangle$ over the 2D Brillouin zone for (a) $n = 0.6$, (b) $n = 0.95$, and (c) $n = 1.3$. We see that the correlator is strongly peaked at $\mathbf{q} = [\pi, \pi]$ near half filling ($n = 1$) due to proximity to the CDW instability and becomes more diffuse as we deviate from half filling on either side. The correlators are calculated from the BdG solutions with $U/t = 3$ and $V/t = 0.1$ and averaged over 15 disorder realizations.

reasonable to only consider the effects of effective static potential fluctuations and neglect the other correlators. We have specifically checked that keeping the other correlators finite does not change the qualitative understanding we get from this simplified assumption. (b) We immediately notice that the correlations are peaked at $\mathbf{Q} = [\pi, \pi]$ for weak disorder. As we increase the disorder strength, the peak at $\mathbf{Q}$ broadens [see Figs. 6(c) and 6(f)], while also increasing in strength. The strong peak at $\mathbf{Q} = [\pi, \pi]$ is due to proximity to the charge density wave (CDW) instability [40] of this model at half filling at the commensurate wave vector. Although we are away from half filling and hence do not have a static CDW order ($\langle \delta v(\mathbf{Q}) \rangle = 0$), the broken translation invariance due to disorder creates strong spatial fluctuations with wave vector $\mathbf{Q}$.

We can tune the system away from the CDW instability by changing the average density away from half filling. In Figs. 7(a)–7(c), we plot $\langle |\delta v(\mathbf{q})|^2 \rangle$ for a system at a fixed weak disorder ($V/t = 0.1$), but with different average densities across half filling [$n = 0.6$ for Fig. 7(a), $n = 0.95$ for Fig. 7(b), and $n = 1.3$ for Fig. 7(c)]. We clearly see that as

we approach half filling, the correlator peaks at $\mathbf{Q}$, while the weight is more diffusely spread over the Brillouin zone as we move away from it. This reinforces the idea that the strong peak at $\mathbf{Q}$ is a signature of the nearby CDW instability in the system. The strong peak of the potential fluctuations around $\mathbf{Q}$ motivates a simpler model where only $\delta v(\mathbf{Q})$ is considered and all other static fluctuations are neglected. In this case, the mode at $\mathbf{q}$ is coupled to the mode at $\mathbf{q} + \mathbf{Q}$, and one can work within a mode coupling theory in a "magnetic Brillouin zone" corresponding to the commensurate wave vector with a doubling of the degrees of freedom. Furthermore, in this case, we will work with the amplitude-phase coordinates for the quantum fluctuation of the superconducting order parameter, i.e., expand $\Delta(r, \tau) = [\Delta_0 + \delta\Delta(r) + \eta(r, \tau)] e^{i\theta(r,\tau)}$, where η and θ are the amplitude and phase of the quantum fluctuations. This allows us to consider the nature of the subgap mode and the partitioning of the subgap weight into the amplitude and phase degrees of freedom cleanly. Within this approximation, the fluctuation action can now be written as

$$S_{fl} = \frac{1}{2} \sum_{\mathbf{q},\omega_m} [\Gamma(\mathbf{q}, i\omega_m), \Gamma(\mathbf{q} - \mathbf{Q}, i\omega_m)] \begin{bmatrix} \hat{D}^{-1}(\mathbf{q}, i\omega_m) & \delta v(\mathbf{Q}) \hat{F}(\mathbf{q}, i\omega_m) \\ \delta v(\mathbf{Q})^* \hat{F}(\mathbf{q} + \mathbf{Q}, i\omega_m) & \hat{D}^{-1}(\mathbf{q} + \mathbf{Q}, i\omega_m) \end{bmatrix} \begin{bmatrix} \Gamma(-\mathbf{q}, -i\omega_m) \\ \Gamma(-\mathbf{q} + \mathbf{Q}, -i\omega_m) \end{bmatrix}, \quad (12)$$

where $\Gamma(\mathbf{q}, i\omega_m) = [\eta(\mathbf{q}, i\omega_m), \theta(\mathbf{q}, i\omega_m), \xi(\mathbf{q}, i\omega_m)]$ is a three-component field containing the amplitude η, the phase θ, and the Hartree potential ξ fluctuations. In some cases, we will suppress the density fluctuations and work with a two-component Γ field. Here, $\hat{D}^{-1}(\mathbf{q}, i\omega_m)$ is the inverse propagator of the quantum fluctuations in the translation-invariant system in the amplitude-phase-potential coordinates,

$$D_{11}^{-1}(\mathbf{q}, i\omega_m) = \frac{1}{U} + \frac{1}{2} \sum_{\mathbf{k}, i\omega_n} \text{Tr}\, {}^N G(\mathbf{k} + \mathbf{q}, i\omega_n + i\omega_m) \sigma^1 G(\mathbf{k}, i\omega_n) \sigma^1,$$

$$D_{12}^{-1}(\mathbf{q}, i\omega_m) = \frac{i}{4}(i\omega_m) \sum_{\mathbf{k}, i\omega_n} \text{Tr}\, {}^N G(\mathbf{k} + \mathbf{q}, i\omega_n + i\omega_m) \sigma^1 G(\mathbf{k}, i\omega_n) \sigma^3 = -D_{12}^{-1}(\mathbf{q}, i\omega_m),$$

$$D_{22}^{-1}(\mathbf{q}, i\omega_m) = (i\omega_m)^2 \kappa(\mathbf{q}, i\omega_m) + \sum_{\hat{\delta} = \pm\hat{x}, \hat{y}} (1 - \cos(\mathbf{q} \cdot \hat{\delta})) \Theta_\delta + \chi(\mathbf{q}, i\omega_m),$$

$$D_{13}^{-1}(\mathbf{q}, i\omega_m) = \frac{1}{2} \sum_{\mathbf{k}, i\omega_n} \text{Tr}^N G(\mathbf{k} + \mathbf{q}, i\omega_n + i\omega_m)\sigma^3 G(\mathbf{k}, i\omega_n)\sigma^1 = D_{31}^{-1}(\mathbf{q}, i\omega_m),$$

$$D_{23}^{-1}(\mathbf{q}, i\omega_m) = -\frac{i}{4}(i\omega_m) \sum_{\mathbf{k}, i\omega_n} \text{Tr}^N G(\mathbf{k} + \mathbf{q}, i\omega_n + i\omega_m)\sigma^3 G(\mathbf{k}, i\omega_n)\sigma^3 = -D_{32}^{-1}(\mathbf{q}, i\omega_m),$$

$$D_{33}^{-1}(\mathbf{q}, i\omega_m) = \frac{1}{U} + \frac{1}{2} \sum_{\mathbf{k}, i\omega_n} \text{Tr}^N G(\mathbf{k} + \mathbf{q}, i\omega_n + i\omega_m)\sigma^3 G(\mathbf{k}, i\omega_n)\sigma^3, \tag{13}$$

where κ is the generalized compressibility, Θ_δ is the kinetic energy, and χ is the current-current correlator in the system given by

$$\kappa(\mathbf{q}, i\omega_m) = \frac{1}{8} \sum_{\mathbf{k}, i\omega_n} \text{Tr}^N G(\mathbf{k} + \mathbf{q}, i\omega_n + i\omega_m)\sigma^3 G(\mathbf{k}, i\omega_n)\sigma^3,$$

$$\Theta_\delta = \frac{t}{2} \sum_{E_\mathbf{k} > 0} v_\mathbf{k}^2 \cos(\mathbf{k} \cdot \hat{\delta}),$$

$$\chi(\mathbf{q}, i\omega_m) = \frac{t^2}{8} \sum_\mathbf{k} (\epsilon_{\mathbf{k}+\mathbf{q}} - \epsilon_\mathbf{k})^2 \sum_{i\omega_n} \text{Tr}^N G(\mathbf{k} + \mathbf{q}, i\omega_n + i\omega_m)\sigma^0 G(\mathbf{k}, i\omega_n)\sigma^0. \tag{14}$$

The details of the D^{-1} matrix derivation are given in the SM [39]. The off-diagonal scattering matrix $\hat{F}$, which gives the amplitude to scatter between $\mathbf{q}$ and $\mathbf{q} + \mathbf{Q}$ modes, is given by

$$F_{11} = \frac{1}{2}\Pi_{113}, \quad F_{21} = -\frac{i}{4}(i\omega_m)\Pi_{313}, \quad F_{12} = \frac{i}{4}(i\omega_m)\Pi_{133}, \quad F_{33} = \frac{1}{2}\Pi_{333},$$

$$F_{13} = \frac{1}{2}\Pi_{133}, \quad F_{23} = -\frac{i}{4}(i\omega_m)\Pi_{333}, \quad F_{31} = -\frac{1}{2}\Pi_{313}, \quad F_{32} = -\frac{i}{4}(i\omega_m)\Pi_{333},$$

$$F_{22} = \frac{(i\omega_m)^2}{8}\Pi_{333} + \frac{1}{8}f_{22}^0 - \left[\frac{(\epsilon_{\mathbf{k}+\mathbf{q}} - \epsilon_\mathbf{k})(\epsilon_\mathbf{k} - \epsilon_{\mathbf{k}+\mathbf{q}+\mathbf{Q}})}{8}\right]\Pi_{003} \tag{15}$$

with

$$[f(\mathbf{k}, \mathbf{q})]\Pi_{abc} = \sum_{\mathbf{k}, i\omega_n} f(\mathbf{k}, \mathbf{q})\text{Tr}^N G(\mathbf{k} + \mathbf{q}, i\omega_n + i\omega_m)\sigma^a G(\mathbf{k}, i\omega_n)\sigma^b G(\mathbf{k} + \mathbf{q} + \mathbf{Q}, i\omega_n + i\omega_m)\sigma^c,$$

$$f_{22}^0 = \sum_{\mathbf{k}, i\omega_n} (\epsilon_{\mathbf{k}+\mathbf{q}} - \epsilon_{\mathbf{k}-\mathbf{q}})\text{Tr}^N G(\mathbf{k}, i\omega_n)\sigma^z G(\mathbf{k} + \mathbf{Q}, i\omega_n)\sigma^z, \tag{16}$$

where Tr^N is the trace over Nambu indices and σ^0 is the identity matrix. One can now invert the full 6×6 inverse propagator matrix to obtain the Green's functions and then construct the spectral functions of the collective bosons. Note that if we are interested in the spectral function of the fluctuations at a fixed $\mathbf{q}$ (as opposed to the matrix element to scatter from $\mathbf{q}$ to $\mathbf{q} + \mathbf{Q}$), the answers only involve $|\delta v(\mathbf{Q})|^2$. We can then replace $|\delta v(\mathbf{Q})|^2$ by its disorder average $\langle|\delta v(\mathbf{Q})|^2\rangle$ and consider the problem as a function of this single parameter. This simplified model, where the effects of disorder have been reduced to a single parameter, contains all the physics behind the systematic changes of the two-particle spectral functions at weak disorder.

A. Collective modes with pairing fluctuations

We first apply our mode coupling model to investigate the collective modes solely in the presence of dynamic pairing fluctuations, i.e., we set the density fields, $\xi(r, \tau) = 0$. In Figs. 8(a) and 8(b) we plot the amplitude spectral function obtained from the mode coupling theory for a system at $n = 0.875$ and $U/t = 3$. Figure 8(a) corresponds to the

clean case, i.e., $\langle|\delta v(\mathbf{Q})|^2\rangle = 0$, while Fig. 8(b) corresponds to $\langle|\delta v(\mathbf{Q})|^2\rangle = 0.01t^2$. The value of $\langle|\delta v(\mathbf{Q})|^2\rangle$ is chosen to be in a realistic regime for systems with weak disorder. In Fig. 8(a), we see the standard collective modes in the homogeneous system, which disperses linearly at low $\mathbf{q}$. The amplitude weight in this mode goes to 0 as $\mathbf{q} \to 0$. In contrast, Fig. 8(b) clearly shows the almost nondispersive weight at finite subgap energy. In the long-wavelength limit, we have a coupling between the zero-energy pure phase Goldstone mode at $\mathbf{q} = [0, 0]$ and the collective mode at $\mathbf{Q}$ (with energy $\omega_\mathbf{Q}$), which has both amplitude and phase components. At weak disorder, the off-diagonal coupling $\delta v_\mathbf{Q} F \ll \omega_\mathbf{Q}$, and hence the finite-frequency spectral weight appears at $\omega_0 \sim \omega_\mathbf{Q} - (\delta v_\mathbf{Q} F)^2/2\omega_\mathbf{Q} \simeq \omega_\mathbf{Q}$. The strong $[\pi, \pi]$ scattering due to the disorder thus creates the narrow subgap weight at $\mathbf{q} = [0, 0]$. Note that as a consequence a mirror image of the mode near [0,0] shows up around $[\pi, \pi]$, which is seen as a pileup in the low-energy spectral weight around the M point. Figures 8(e) and 8(f) show the phase spectral functions corresponding to the amplitude spectral functions shown in Figs. 8(a) and 8(b), respectively. We note that the subgap mode, in this case, shows up both in the amplitude and phase spectral functions.
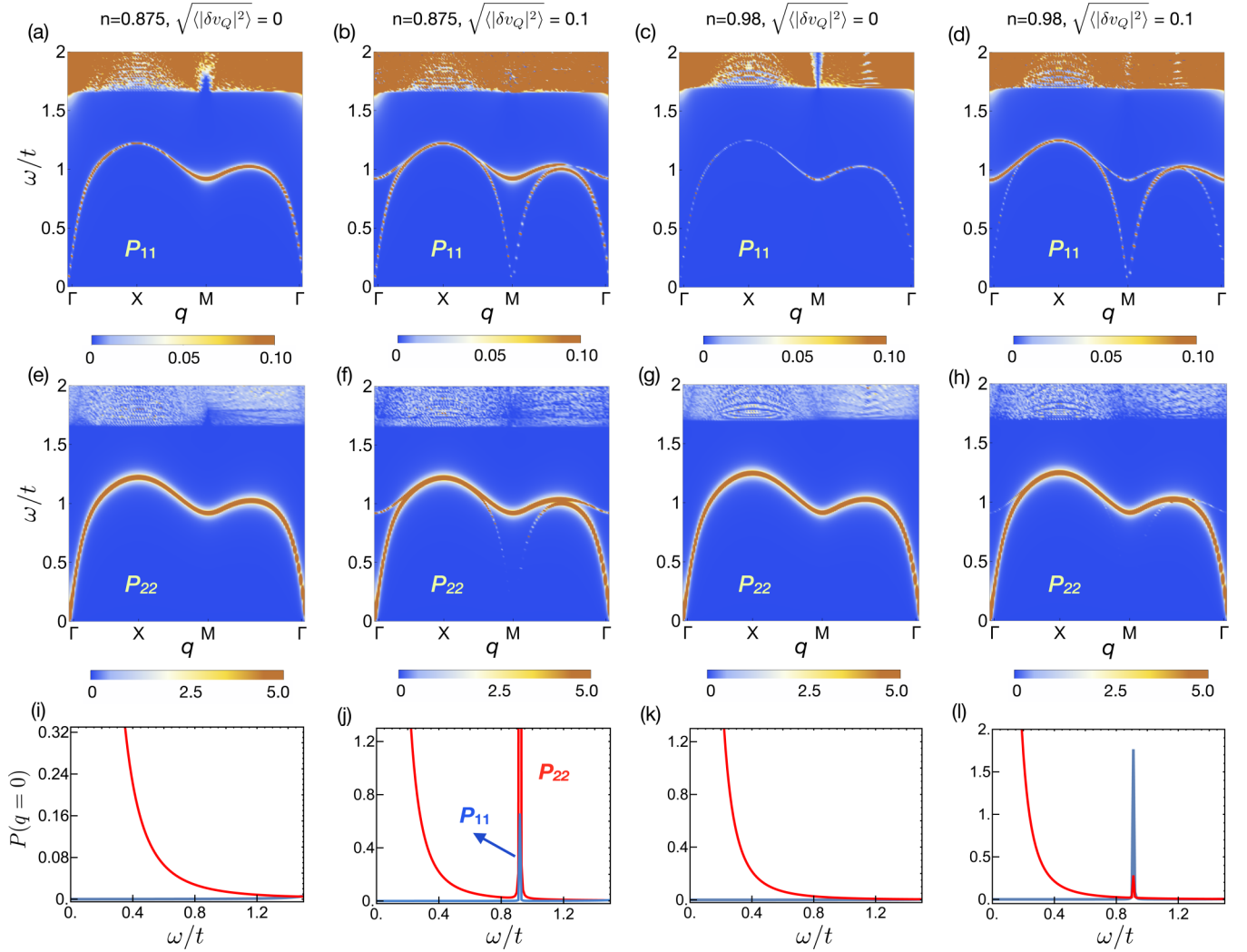
FIG. 8. Results from the mode coupling theory. (a) and (b) show the amplitude spectral functions P_{11} for $n = 0.875$. (a) corresponds to the clean case $\sqrt{\langle |\delta v(\mathbf{Q})|^2 \rangle} = 0$, while (b) corresponds to a weak disorder with $\sqrt{\langle |\delta v(\mathbf{Q})|^2 \rangle} = 0.1 t$. (c) and (d) are similar to (a) and (b), respectively, but for $n = 0.98$. The subgap mode is clearly visible for the disordered case for both $n = 0.875$ (b) and $n = 0.98$ (d). The phase spectral functions P_{22} corresponding to the cases in (a)–(d) are plotted in (e)–(h), respectively. The subgap mode is clearly seen at $n = 0.875$ (f), while it is strongly suppressed at $n = 0.98$ (h). Moreover, the phase channel is suppressed close to half filling. The EDCs at $\mathbf{q} = [0, 0]$ for the amplitude (blue) and phase (red) spectral functions for the cases corresponding to (a)–(d) are plotted in (i)–(l), respectively. All the plots have a low-energy tail from the pure phase Goldstone mode. In the disordered cases shown in (j) and (l), the subgap mode is clearly seen. At $n = 0.98$ close to half filling the subgap weight is dominated by the amplitude component, while at $n = 0.875$ away from half filling the phase component dominates. The calculations are done on a 100×100 lattice. The single-particle gaps of the clean superconductors are $\Delta_0/t = 0.85, 0.83$ for $n = 0.98, 0.875$, respectively.

Figures 8(i) and 8(j) show the energy distribution curves at $\mathbf{q} = [0, 0]$ for the clean and the disordered cases, respectively. In the clean case [Fig. 8(i)], one can clearly see that there is no subgap Higgs weight, while the low-energy phase weight gets a contribution from the Goldstone mode. In contrast, in Fig. 8(j), the disorder scattering creates additional spectral weight in the amplitude and phase channels at approximately the energy of the homogeneous collective mode at $\mathbf{Q}$. This weight is narrowly distributed in energy and is well separated from the low-energy collective mode weight. We note that in a real disordered system, the disorder scattering happens with all momentum transfers, with the scattering amplitude peaking at $\mathbf{Q}$. In this case, one would expect the spectral weight

to be smeared over a larger energy window. Furthermore, as the scattering becomes diffuse with increasing disorder, one would expect this mode to broaden, which is what is seen in the numerics around the disordered inhomogeneous BdG saddle point.

We now focus on the amplitude and phase components of the spectral weight at $\mathbf{q} = [0, 0]$ at finite frequency. In the numerical results, we have seen that as we move away from half filling the phase component of the spectral weight increases at the expense of the amplitude. To understand this trend, we consider the scattering matrix $\hat{F}(\mathbf{Q}, i\omega_m)$ at the particle-hole-symmetric half-filling limit, where the chemical potential $\mu - v_0 = 0$. Using the fact that $\epsilon_{\mathbf{k}+\mathbf{Q}} = -\epsilon_{\mathbf{k}}$ and

$G(\mathbf{k} + \mathbf{Q}) = \sigma^1 G(\mathbf{k})\sigma^1$, one can show that

$$F_{11}(\mathbf{Q}, i\omega_m) = \sum_{\mathbf{k}} \frac{\epsilon_{\mathbf{k}}}{E_{\mathbf{k}}} \frac{1}{(i\omega_m)^2 - 4E_{\mathbf{k}}^2} = 0,$$

$$F_{12}(\mathbf{Q}, i\omega_m) = -\frac{i}{2}(i\omega_m) \sum_{\mathbf{k}} \frac{\Delta}{E_{\mathbf{k}}} \frac{1}{(i\omega_m)^2 - 4E_{\mathbf{k}}^2},$$

$$F_{22}(\mathbf{Q}, i\omega_m) = -\frac{(i\omega_m)^2}{4} \sum_{\mathbf{k}} \frac{\epsilon_{\mathbf{k}}}{E_{\mathbf{k}}} \frac{1}{(i\omega_m)^2 - 4E_{\mathbf{k}}^2} = 0. \quad (17)$$

Here, $F_{21}(\mathbf{Q}, i\omega_m) = -F_{12}(\mathbf{Q}, i\omega_m)$. We note that the $\mathbf{q} = [0, 0]$ mode is always a pure phase mode. Since particle-hole symmetry prohibits a coupling between the phase component at $\mathbf{q} = [0, 0]$ and the phase component at $\mathbf{q} = [\pi, \pi]$ ($F_{22} = 0$) at half filling, the Goldstone mode primarily couples to the amplitude component of the $[\pi, \pi]$ mode near half filling. Hence, in the weak-disorder limit, when the off-diagonal coupling between the modes is much smaller than $\omega_{\mathbf{Q}}$, the finite-frequency weight is mostly in the amplitude channel. To see this, we plot the two-particle spectral function for a system with $n = 0.98$ close to half filling at a weak disorder of $\langle|\delta v(\mathbf{Q})|^2\rangle = 0.01t^2$ in Fig. 8(d) (amplitude spectral function) and Fig. 8(h) (phase spectral function), respectively. The corresponding clean case spectral functions are shown in Figs. 8(c) and 8(g), respectively. In this case we can clearly see that at $\mathbf{q} = [0, 0]$, the finite-frequency subgap spectral weight is seen mostly in the amplitude channel, while the phase spectral weight is concentrated near $\omega = 0$. This is clearly illustrated in the energy distribution cuts (at $\mathbf{q} = [0, 0]$ in Fig. 8(k) (clean case) and Fig. 8(l) (at weak disorder)). In Fig. 8(l), we clearly see a finite subgap weight dominated by the Higgs channel, which is spectrally separated from the low-energy weight in the phase channel. As one moves away from the half filling, F_{22} increases, and hence the phase component of the finite-frequency spectral weight increases, as seen in the more accurate numerical calculations shown in Sec. II.

We note that while our simplified toy model of mode coupling correctly predicts the trends, it does not provide quantitatively correct answers; for example, at $n = 0.875$, the numerical calculations show a preponderance of amplitude spectral weight, while we need to go much closer to half filling ($n = 0.98$) to see this. Thus the mode coupling theory should be used to understand systematic trends and should not be used to directly compare quantitatively with the numerical results. However, it still provides valuable insights into the mechanisms behind the systematic trends, which are hard to obtain from more sophisticated calculations.

B. Effects of density fluctuations

We have so far considered the quantum fluctuations in the superconducting order parameter to determine the collective mode spectrum, while the Hartree field was accounted for only through its static fluctuations, i.e., the standard deviation of its spatial variations in the inhomogeneous mean-field solutions. We now consider the effects of dynamic density fluctuations on the two-particle spectral weight by considering

$$\xi(r) \rightarrow \xi_0 + \delta v(r) + \xi(r, \tau),$$
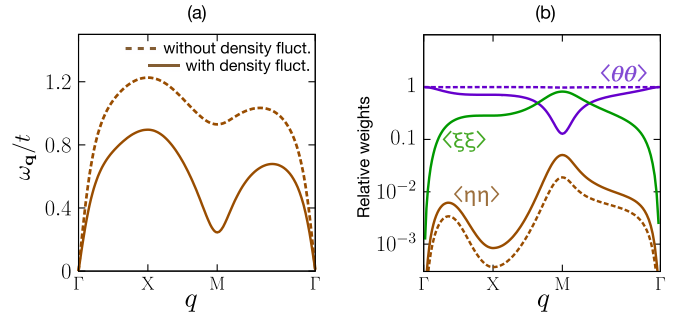
FIG. 9. (a) The collective mode dispersion of a clean *s*-wave superconductor with (solid lines) and without (dashed lines) density fluctuation at $U/t = 3$ and $n = 0.875$. The inclusion of density fluctuations lowers the collective mode frequency near the *M* point substantially. (b) The relative weight of the amplitude (brown), phase (purple), and density (green) fluctuations in the collective modes is shown. Near the *M* point there is a transfer of weight from the phase to the density channel.

where ξ represent the temporally and spatially varying particle-hole fluctuations. We note that this is a key difference between the approximations made in Ref. [23] and those made in Ref. [24]; those papers reach different conclusions on the exact location of the subgap weight and its amplitude-phase distribution. Compared with Refs. [23,24] finds broad subgap weights at lower frequencies, with much larger phase spectral weight. Before we consider the mode coupling theory due to disorder scattering, we first consider how the collective mode in the uniform system changes due to inclusion of these density fluctuations, i.e., set $\langle|\delta v(\mathbf{Q})|^2\rangle = 0$.

In this case, Γ is a three-component vector, and the collective modes can be found from the zeros of the determinant of the 3×3 matrix that forms the inverse propagator for the fluctuations. In Fig. 9(a), we plot the dispersion of the collective modes in a clean system (at $U/t = 3$, $n = 0.875$) calculated with (solid line) and without (dashed line) considering the density fluctuations. The main effect of including the density fluctuations is to lower the collective mode frequency at large $\mathbf{q}$, especially around the *M* point. This is once again due to the proximity of the CDW instability. At the CDW instability, one expects the collective mode frequency to go to 0 at the *M* point. We note that one can integrate out the density fluctuations to obtain an effective amplitude-phase correlator, but the collective mode dispersion remains essentially the same whether one works with a 3×3 propagator or an effective 2×2 propagator. In Fig. 9(b), we plot the relative weights of the amplitude, phase, and density sectors in the collective modes (by considering the eigenvector which gives the collective mode). We see that the weight of the amplitude sector is almost unaffected by inclusion of the density fluctuations. In the long-wavelength limit, the weight of the density fluctuations goes to zero. The main effect of the density fluctuations can be seen near $M = [\pi, \pi]$, where the weight is transferred from the phase to the density channel.

We now consider the effects of density fluctuations on the spectral functions in the disordered system through the mode coupling theory. In Figs. 10(a) and 10(b) we plot the amplitude spectral function of a system at $U/t = 3$ and $n = 0.875$
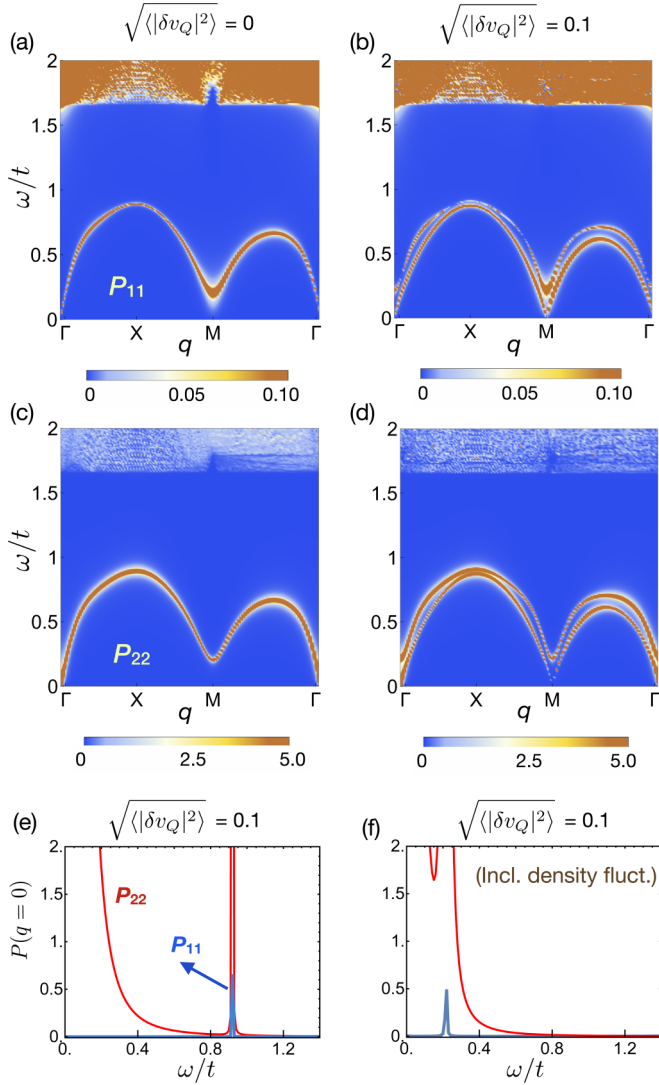
FIG. 10. (a) and (b) The amplitude spectral fluctuations and (c) and (d) the phase spectral functions calculated using the mode coupling theory including the effects of density fluctuations. (a) and (c) correspond to the clean case, while (b) and (d) correspond to the weak disorder with $\sqrt{\langle|\delta v(\mathbf{Q})|^2\rangle} = 0.1t$. (e) and (f) show the EDC at $\mathbf{q} = [0, 0]$ both (e) without and (f) with density fluctuations at a weak disorder of $\sqrt{\langle|\delta v(\mathbf{Q})|^2\rangle} = 0.1t$. Including density fluctuations causes the subgap mode at $\mathbf{q} = [0, 0]$ to shift to a lower frequency and increases the relative contribution of the phase mode. The calculations were done within mode coupling theory at $U/t = 3$ and $n = 0.875$ on a 100×100 lattice. The single-particle gap of the corresponding clean superconductor is $\Delta_0/t = 0.83$.

for the clean case ($\langle|\delta v(\mathbf{q})|^2\rangle = 0$) and for a weak disorder ($\langle|\delta v(\mathbf{q})|^2\rangle = 0.1$), respectively. Figures 10(c) and 10(d) show the corresponding phase spectral functions. While the amplitude spectral function is almost unchanged, we clearly see two split bands in the phase spectral function. Figure 10(e) shows the spectral function at $\mathbf{q} = [0, 0]$ as a function of energy for the disordered system in the absence of dynamic density fluctuations, while Fig. 10(f) shows the same quantity when these fluctuations are included. Two trends are clearly seen: (i) The additional feature at finite frequencies is pushed

down when density fluctuations are included. Within the mode coupling theory, as the collective mode frequency at $\mathbf{Q}$ comes down, it pushes the additional feature at $\mathbf{q} = [0, 0]$ downwards. Note that a sharp additional feature can be seen in this case with identifiable amplitude and phase contributions, although it is no longer spectrally separated from the tail of the spectral weight from the zero-energy Goldstone mode. In a theory where scattering at all momenta is kept, this feature will be broadened further. (ii) The additional feature has a much larger phase component compared with the case without density fluctuations. We note that since the energy of the mode at $\mathbf{Q}$ is smaller in this case, there is a larger mixing between the $\mathbf{q} = [0, 0]$ Goldstone mode (which is a pure phase mode) and the mode at $[\pi, \pi]$, leading to a larger phase component in the subgap weight. Thus our two-mode model is able to accurately capture this trend and can also resolve the discrepancies between Refs. [23,24].

V. CONCLUSION

In this paper we have shown that the collective modes and two-particle spectral weight of a weakly disordered superconductor can be obtained from a model where the translation-invariant collective modes are scattered by an effective disorder. Starting with a microscopic theory of attractive fermions in the presence of random potential disorder, we construct this effective theory by expanding the action around a translation-invariant saddle point in both the static spatial fluctuations induced by disorder and the dynamic quantum fluctuations. We can thus construct the parameters of this effective model starting from a fermionic theory. We show that a simple Born approximation for the disorder scattering of the collective modes reproduces the long-wavelength ($\mathbf{q} = [0, 0]$) subgap spectral weight at finite frequencies, which have been seen earlier in numerical calculations around the inhomogeneous BdG mean-field solution.

In the attractive Hubbard model on a square lattice, the system undergoes a CDW instability with $\mathbf{Q} = [\pi, \pi]$ at half filling. In the presence of disorder, there are strong static fluctuations of density and pairing fields at this commensurate wave vector, even when the system is away from half filling. Such strong fluctuations will be a generic feature of systems near a CDW instability. The effective disorder seen by the collective modes thus shows a strong peak at this wave vector. This leads to a simple mode coupling theory (coupled by random static fluctuations), which provides analytic insight into the subgap weight in the two-particle spectral functions at $\mathbf{q} = [0, 0]$ and captures the trends seen in the numerical calculations. The subgap weight is formed by disorder scattering of the $[\pi, \pi]$ mode and appears around the energy of this collective mode. The particle-hole symmetry at half filling ensures that this mode consists primarily of amplitude fluctuations near half filling. As we move away in density, the phase contribution to this mode increases. Including dynamic density fluctuations lowers the frequency of the $[\pi, \pi]$ mode substantially, and hence the spectral separation between the tail of the Goldstone weight and this mode is lost. The lower frequency also implies a larger mixing of the $\mathbf{q} = [0, 0]$ Goldstone mode (which is a pure phase mode), and hence the phase

contribution to the subgap weight increases substantially in this case.

We have thus obtained a generic framework to obtain the two-particle spectral weight of weakly disordered superconductors. Therefore, close to a CDW transition, we obtain a simpler mode coupling theory. The trends explain the discrepancies between Refs. [23,24]. The extension of this framework to stronger disorder strengths by going beyond the simple Born approximation is left for future work.

[1] G. Kopnov, O. Cohen, M. Ovadia, K. H. Lee, C. C. Wong, and D. Shahar, Phys. Rev. Lett. **109**, 167002 (2012).

[2] B. Sacépé, T. Dubouchet, C. Chapelier, M. Sanquer, M. Ovadia, D. Shahar, M. Feigel'Man, and L. Ioffe, Nat. Phys. **7**, 239 (2011).

[3] Y. Dubi, Y. Meir, and Y. Avishai, Nature (London) **449**, 876 (2007).

[4] M. Chand, G. Saraswat, A. Kamlapure, M. Mondal, S. Kumar, J. Jesudasan, V. Bagwe, L. Benfatto, V. Tripathi, and P. Raychaudhuri, Phys. Rev. B **85**, 014508 (2012).

[5] A. Ghosal, M. Randeria, and N. Trivedi, Phys. Rev. B **65**, 014501 (2001).

[6] K. Bouadim, Y. L. Loh, M. Randeria, and N. Trivedi, Nat. Phys. **7**, 884 (2011).

[7] N. Trivedi, R. T. Scalettar, and M. Randeria, Phys. Rev. B **54**, R3756 (1996).

[8] G. Sambandamurthy, L. Engel, A. Johansson, and D. Shahar, Phys. Rev. Lett. **92**, 107005 (2004).

[9] R. Shimano and N. Tsuji, Annu. Rev. Condens. Matter Phys. **11**, 103 (2020).

[10] D. Pekker and C. Varma, Annu. Rev. Condens. Matter Phys. **6**, 269 (2015).

[11] G. Aad, T. Abajyan, B. Abbott, J. Abdallah, S. A. Khalek, A. A. Abdelalim, R. Aben, B. Abi, M. Abolins, O. AbouZeid, H. Abramowicz, H. Abreu, B. S. Acharya, L. Adamczyk, D. L. Adams, T. N. Addy, J. Adelman, S. Adomeit, P. Adragna, T. Adye *et al.* (ATLAS Collaboration), Phys. Lett. B **716**, 1 (2012).

[12] R. Matsunaga, Y. I. Hamada, K. Makise, Y. Uzawa, H. Terai, Z. Wang, and R. Shimano, Phys. Rev. Lett. **111**, 057002 (2013).

[13] R. Matsunaga, N. Tsuji, H. Fujita, A. Sugioka, K. Makise, Y. Uzawa, H. Terai, Z. Wang, H. Aoki, and R. Shimano, Science **345**, 1145 (2014).

[14] R. Matsunaga, N. Tsuji, K. Makise, H. Terai, H. Aoki, and R. Shimano, Phys. Rev. B **96**, 020505(R) (2017).

[15] T. Cea, C. Castellani, and L. Benfatto, Phys. Rev. B **93**, 180507(R) (2016).

[16] G. Seibold, M. Udina, C. Castellani, and L. Benfatto, Phys. Rev. B **103**, 014512 (2021).

[17] H. Chu, M.-J. Kim, K. Katsumi, S. Kovalev, R. D. Dawson, L. Schwarz, N. Yoshikawa, G. Kim, D. Putzky, Z. Z. Li, H. Raffy, S. Germanskiy, J.-C. Deinert, N. Awari, I. Ilyakov, B. Green, M. Chen, M. Bawatna, G. Cristiani, G. Logvenov *et al.*, Nat. Commun. **11**, 1793 (2020).

[18] L. Schwarz, B. Fauseweh, and D. Manske, Phys. Rev. B **101**, 224510 (2020).

[19] D. Sherman, U. S. Pracht, B. Gorshunov, S. Poran, J. Jesudasan, M. Chand, P. Raychaudhuri, M. Swanson, N. Trivedi, A. Auerbach, M. Scheffler, A. Frydman, and M. Dressel, Nat. Phys. **11**, 188 (2015).

[20] P. Littlewood and C. Varma, Phys. Rev. B **26**, 4883 (1982).

[21] J. R. Engelbrecht, M. Randeria, and C. S. Melo, Phys. Rev. B **55**, 15153 (1997).

[22] R. B. Diener, R. Sensarma, and M. Randeria, Phys. Rev. A **77**, 023626 (2008).

[23] A. Samanta, A. Ratnakar, N. Trivedi, and R. Sensarma, Phys. Rev. B **101**, 024507 (2020).

[24] T. Cea, C. Castellani, G. Seibold, and L. Benfatto, Phys. Rev. Lett. **115**, 157002 (2015).

[25] T. Cea and L. Benfatto, Phys. Rev. B **90**, 224515 (2014).

[26] A. Samanta, A. Das, N. Trivedi, and R. Sensarma, Phys. Rev. B **105**, 104503 (2022).

[27] T. Xiang and J. Wheatley, Phys. Rev. B **51**, 11721 (1995).

[28] W. Atkinson, P. Hirschfeld, and A. MacDonald, Phys. Rev. Lett. **85**, 3922 (2000).

[29] C. J. Arguello, S. P. Chockalingam, E. P. Rosenthal, L. Zhao, C. Gutiérrez, J. H. Kang, W. C. Chung, R. M. Fernandes, S. Jia, A. J. Millis, R. J. Cava, and A. N. Pasupathy, Phys. Rev. B **89**, 235115 (2014).

[30] P. W. Anderson, Phys. Rev. **110**, 827 (1958).

[31] P. W. Anderson, Phys. Rev. **112**, 1900 (1958).

[32] A. M. Finkel'stein, Phys. B (Amsterdam) **197**, 636 (1994).

[33] P. W. Anderson, Phys. Rev. **130**, 439 (1963).

[34] V. Dobrosavljevic, N. Trivedi, and J. M. Valles, Jr., *Conductor-Insulator Quantum Phase Transitions* (Oxford University Press, Oxford, UK, 2012), Chap. 17, pp. 492–548.

[35] D. Chakraborty, R. Sensarma, and A. Ghosal, Phys. Rev. B **95**, 014516 (2017).

[36] A. Datta, A. Banerjee, N. Trivedi, and A. Ghosal, arXiv:2101.00220 [cond-mat.supr-con].

[37] T. Baturina, C. Strunk, M. Baklanov, and A. Satta, Phys. Rev. Lett. **98**, 127003 (2007).

[38] M. Steiner and A. Kapitulnik, Phys. C (Amsterdam) **422**, 16 (2005).

[39] See Supplemental Material at http://link.aps.org/supplemental/10.1103/PhysRevB.106.064512 for the detailed evaluation of M^{-1}, the explicit evaluation of the coupling functions $f_{\alpha\beta}$ and $g_{\alpha\beta}$, and details of the D^{-1} matrix derivation.

[40] A. Auerbach, *Interacting Electrons and Quantum Magnetism* (Springer, New York, 2012).